UACJ Technical Reports, Vol.1 (2014), pp. 8-16

論　文

Influence of Silicon on Intergranular Corrosion for Aluminum Alloy*

Yoshiyuki Oya** and Yoichi Kojima**

An alternative fluorocarbon refrigerant of a heat exchanger of a car air conditioner may change to carbon dioxide refrigerant which has lower global warming potential than the alternative fluorocarbon refrigerant. If carbon dioxide is used as a refrigerant, both pressure and temperature of a heat exchanger will become higher. Silicon is a potential element added to aluminum to use for the heat exchangers with carbon dioxide refrigerant because of increase in tensile strength. The operation temperature affects metallographic structure of aluminum-silicon alloy, might leading to intergranular corrosion. To investigate influence of Si concentration and heat treatment at 453 K on susceptibility to intergranular corrosion, in various alloys, electrochemical measurements and observation of the metal textures were performed. The susceptibility to intergranular corrosion increased with increase in Si concentration and increased with heat treatment time at 453 K once, but turned to decrease by long term heat treatment at 453 K. Addition of Mg and Mn promoted generation and disappearance of susceptibility to intergranular corrosion in Al-Si alloy. Si precipitates were observed by TEM. Without and with short heat treatment at 453 K, small Si precipitates were observed on grain boundary and could not observe precipitate in grain. With long heat treatment at 453 K, large Si precipitates were observed in grains and on grain boundaries. Short heat treatment at 453 K formed continuous Si depleted layer along grain boundaries. The Si depleted layer increased susceptibility to intergranular corrosion. However, long heat treatment at 453 K decreased the susceptibility to intergranular corrosion. Addition of Mg and Mn affects precipitation of Si precipitates. It is suggested that the susceptibility to intergranular corrosion had dependence of addition of Mg and Mn.

Keywords: *aluminum alloy, intergranular corrosion, brazing process, heat treatment*

1. Introduction

Aluminum-manganese (Al-Mn) series aluminum alloys which are representative as 3003 and 3203 alloy are widely used for materials of heat exchangers because of high tensile strength and corrosion resistance. Heat exchangers in car air conditioners are produced by a brazing process and CFC-134a (CH_2FCF_3) is used as refrigerant. The refrigerant may change to carbon dioxide (CO_2) which has lower global warming potential than the alternative fluorocarbon refrigerant[1]. If CO_2 is used as the refrigerant, both pressure and temperature in the heat exchanger would become higher. Copper (Cu) and silicon (Si) are often added to Al-Mn series aluminum alloys for increasing in tensile strength. However, when the high strength Al-Mn series aluminum alloys with Cu and Si are applied to the heat exchanger with the CO_2 refrigerant, solute elements are precipitated preferentially on a grain boundary because the operation temperature reaches to 453 K[1]. The precipitation induces the concentration difference between the grain and grain boundaries, might leading to intergranular corrosion.

Al-Mn series aluminum alloys have comparatively low susceptibility to intergranular corrosion although the susceptibility increases due to heat treatment and addition of alloy elements[2)-4)]. The heat treatment such

* This paper is reprinted from Mater. Trans. **54** (2013), 1200-1208

** No. 2 Department, Fukaya Center, Research & Development Division, UACJ Corporation

as at more than 673 K at which Al_6Mn and/or $Al_6(MnFe)$ precipitate preferentially on grain boundaries forms Mn depleted layer along grain boundaries. Preferential corrosion of the Mn depleted layer causes the intergranular corrosion. In an Al-Mn alloy Cu as an alloy element and iron (Fe) as an impurity enhanced susceptibility to intergranular corrosion[2), 3)] but Si inhibited susceptibility to intergranular corrosion[4)].

A mechanism about generation of intergranular corrosion has been investigated carefully for Al-Cu alloys[5)]. Heat treatment at which Al_2Cu intermetallic compound precipitates on grain boundaries preferentially forms Cu depleted layer along grain boundaries. This is reason why the diffusion rate of Cu on grain boundaries is higher than that in grains. Since solute Cu makes pitting potential (E_{PIT}) of aluminum alloy noble, E_{PIT} of the grain boundary is lower than that of the grains. Difference in E_{PIT} between the grain and grain boundary causes intergranular corrosion. Thus, it means that addition of Cu in aluminum alloy is harmful for the intergranular corrosion. However, tensile strength of Al-Mn alloys without Cu is intolerably low for usage of the heat exchanger with CO_2 refrigerant. Addition of other elements to increase tensile strength is imperative.

Si is a major element added to aluminum alloy. Si in aluminum alloy contributes to increase tensile strength due to solid solution and precipitation strengthening. The precipitation of the various intermetallic compounds containing Si was affected by heat treatment meaning that susceptibility to intergranular corrosion also changed[6)-11)]. The intergranular corrosion was not observed for water quenched Al-Si[8)] and Al-Si-Mg[6), 7), 9)] alloys but was observed for air cooled Al-Si[8)], Al-Si-Mg[6), 10)] and Al-Si-Mn[11)]. Heat treatment increased in susceptibility to intergranular corrosion for Al-Si-Mg[6), 7), 9)] and Al-Si-Mn[10), 11)]. These intergranular corrosion were caused by dissolution of Mg_2Si intermetallic compound on grain boundary in Al-Si-Mg[7), 9)] or Si depleted layer along grain boundary in Al-Si and Al-Mn-Si alloys[6), 8), 10), 11)]. It means that the cause of the intergranular corrosion depended on the type of alloys. However, there are few reports about systematic study about influence of Si concentration in various alloys and heat treatment conditions on susceptibility to intergranular corrosion. In this study, it is investigated that Si concentration and heat treatment time at 453 K after brazing process affect the susceptibility to intergranular corrosion using various alloys.

2. Experimental Procedure

2.1 Process and materials

Chemical compositions of specimens are shown in **Table 1**. All specimens were cast in book mold, homogenized at 873 K for 1.08×10^4 s, hot rolled at 793 K to 3.5 mm thickness, and then cold rolled to 1 mm thickness. The sheets were annealed at 673 K for 7.20×10^3 s. The annealed sheets were heat-treated at 873 K for 180 s which corresponded to a brazing process. Finally, the brazed sheets were reheated at 453 K which is the maximum working temperature for CO_2 air conditioners for $0 - 7.20 \times 10^6$ s. The heat-treated time at 453 K after brazing process is regarded as HTT (t_{HT}) in this paper.

2.2 TEM observation

Distribution of precipitated intermetallic compounds near grain boundaries of the specimens heat-treated at 453 K was observed by TEM (JEOL Ltd., JEM-3100FEF, accelerating voltage: 300 kV).

2.3 Evaluations of susceptibility to intergranular corrosion

Susceptibility to intergranular corrosion was evaluated by anodic dissolution. A Pt plate was used as a counter electrode. Test solution was 5mass%

Table 1 Chemical compositions of specimens. (mass%)

	Si	Fe	Cu	Mn	Mg	Al
0.4Si	0.4	0.4	0	0	0	Bal.
0.8Si	0.8	0.4	0	0	0	Bal.
1.2Si	1.2	0.4	0	0	0	Bal.
1.4Si	1.4	0.4	0	0	0	Bal.
0.2Mg-0.9Si	0.9	0.4	0	0	0.2	Bal.
0.2Mg-1.3Si	1.3	0.4	0	0	0.2	Bal.
1.1Mn-0.4Si	0.4	0.4	0	1.1	0	Bal.
1.1Mn-0.8Si	0.8	0.4	0	1.1	0	Bal.
1.1Mn-1.2Si	1.2	0.4	0	1.1	0	Bal.
1.1Mn-1.4Si	1.4	0.4	0	1.1	0	Bal.
1.1Mn-0.2Mg-0.6Si	0.6	0.4	0	1.1	0.2	Bal.
1.1Mn-0.2Mg-0.8Si	0.8	0.4	0	1.1	0.2	Bal.
1.1Mn-0.2Mg-1.2Si	1.2	0.4	0	1.1	0.2	Bal.
1.1Mn-0.2Mg-1.4Si	1.4	0.4	0	1.1	0.2	Bal.

(after this, mass% is shortened to %) NaCl adjusted pH to 3 by acetic acid. The specimens were immersed in 5% NaOH at 333 K for 30 s, rinsed with distilled water, immersed in a 30% HNO_3 at 298 K for 60 s and then rinsed with distilled water as a pretreatment. Applied anodic current density was 10 Am^{-2} at which the specimens were polarized to the potential which is higher than E_{PIT}. The polarization time is 2.16×10^4 s. After the anodic dissolution, cross section of the center of the specimen with optical microscope was observed for identifying corrosion morphology and measuring corrosion depth. In this paper, the corrosion depth means the maximum depth from surface to the bottom of corrosion in observed 30 views.

3. Results

3.1 Al-Si alloys

3.1.1 Susceptibility to intergranular corrosion

Fig. 1 shows optical micrographs of the cross section after anodic dissolution for 0.4Si, 0.8Si, and 1.2Si at t_{HT} = 0, 8.64×10^4 and 2.59×10^6 s. At t_{HT} = 0 s, corrosion morphology depended on Si concentration. Pitting corrosion was observed for 0.4Si and 0.8Si and intergranular corrosion was observed for 1.2Si. At t_{HT} = 8.64×10^4 s, pitting corrosion was observed for 0.4Si, while intergranular corrosion was observed for 0.8Si and 1.2Si. The corrosion depth at t_{HT} = 8.64×10^4 s was deeper than that at t_{HT} = 0 s. Corrosion morphology was independent of Si concentration, being pitting corrosion at t_{HT} = 2.59×10^6 s.

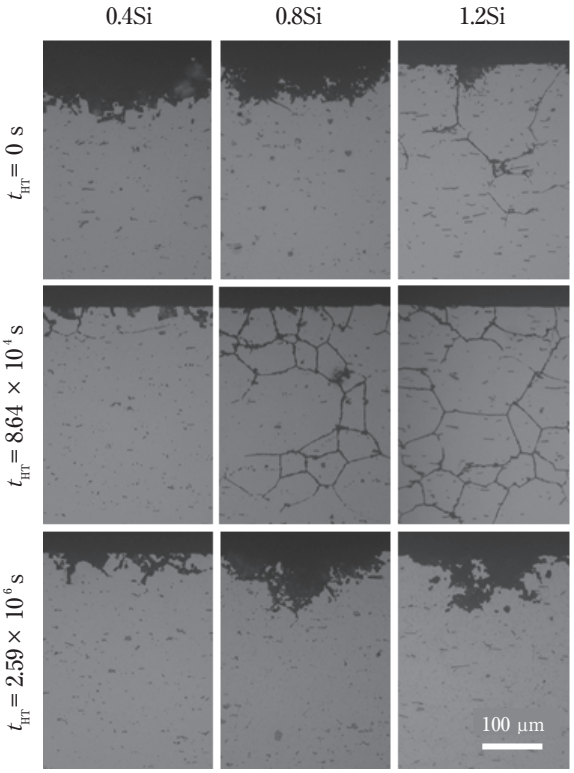

Fig. 1 Optical micrographs of the cross section after anodic dissolution for 0.4Si, 0.8Si, and 1.2Si at t_{HT} = 0, 8.64×10^4 and 2.59×10^6 s.

Fig. 2 shows relationships between HTT and corrosion depth for 0.4Si, 0.8Si, 1.2Si, and 1.4Si. The open and solid symbols show pitting corrosion and intergranular corrosion, respectively. If the current efficiency is constant in anodic dissolution regardless of corrosion morphology, the volume of dissolved aluminum is constant in anodic dissolution applying constant current density, the corrosion depth would show a tendency of intergranular corrosion. The corrosion depth of 0.4Si was independent of HTT, being about 5.0×10^{-5} m. The corrosion morphology of 0.4Si is pitting corrosion. The corrosion depth and morphology of 0.8Si, 1.2Si, and 1.4Si depended on HTT. For 0.8Si, corrosion morphology was pitting corrosion at t_{HT} = 0 s. Corrosion depth increased at 0 ≤ t_{HT} ≤ 8.64×10^4 s although the intergranular corrosion was observed at $7.20 \times 10^3 \le t_{HT} \le 6.05 \times 10^5$ s. Furthermore, the corrosion morphology was pitting corrosion again at t_{HT} = 2.59×10^6 s. For 1.2Si and 1.4Si, intergranular corrosion was observed at t_{HT} = 0 – 6.05×10^5 s, corrosion morphology was pitting

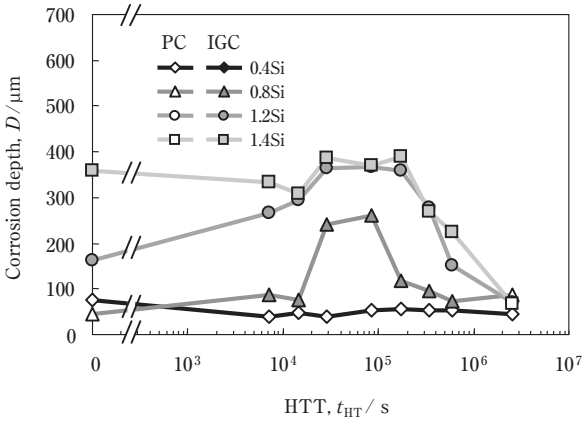

Fig. 2 Relationships between HTT and corrosion depth for 0.4Si, 0.8Si, 1.2Si, and 1.4Si. Pitting corrosion and intergranular corrosion are denoted as PC and IGC, respectively.

corrosion at $t_{HT} = 2.59 \times 10^6$ s. Corrosion depth was the deepest at $t_{HT} = 8.64 \times 10^4$ or 1.73×10^5 s and then decreased rapidly with increase in HTT. That is, susceptibility to intergranular corrosion showed peak at $t_{HT} = 8.64 \times 10^4$ s for 0.8Si and 1.2Si and at $t_{HT} = 1.73 \times 10^5$ s for 1.4Si.

3.1.2 TEM observation

Fig. 3 shows bright field TEM images of precipitates on grain boundaries for 1.2Si at $t_{HT} = 0$ and 2.59×10^6 s. At $t_{HT} = 0$ s, Si precipitates with diameter of about 1×10^{-7} m were observed on grain boundaries and could not be observed in grain. On the other hand, Si precipitates with diameter of about 1×10^{-5} m were observed in grains and on grain boundaries at $t_{HT} = 2.59 \times 10^6$ s. This indicates that precipitation and growth of Si precipitates occurred by the heat treatment at 453 K.

3.2 Al-0.2%Mg-Si alloys

3.2.1 Susceptibility to intergranular corrosion

Fig. 4 shows optical micrographs of the cross section after anodic dissolution for 0.2Mg-0.9Si and -1.3Si at $t_{HT} = 0$, 8.64×10^4, and 2.59×10^6 s. Corrosion morphology depended on Si concentration at $t_{HT} = 0$ s. Pitting corrosion was observed for 0.2Mg-0.9Si and intergranular corrosion was observed for 0.2Mg-1.3Si. At $t_{HT} = 8.64 \times 10^4$ s, obvious intergranular corrosion was observed for 0.2Mg-0.9Si and corrosion morphology was pitting corrosion for 0.2Mg-1.3Si. At $t_{HT} = 2.59 \times 10^6$ s, corrosion morphology was pitting corrosion in each Si concentration.

Fig. 5 shows relationships between HTT and the corrosion depth for 0.2Mg-0.9Si and -1.3Si. The open

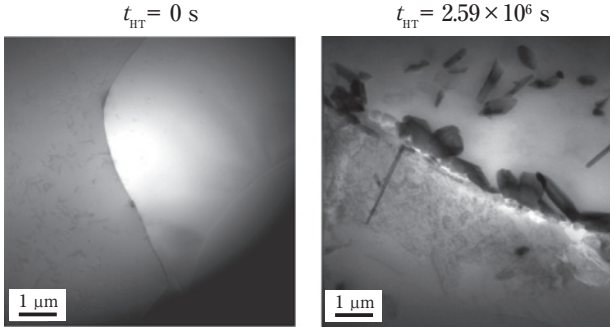

Fig. 3 Bright field TEM images of precipitates on grain boundaries for 1.2Si at $t_{HT} = 0$ and 2.59×10^6 s.

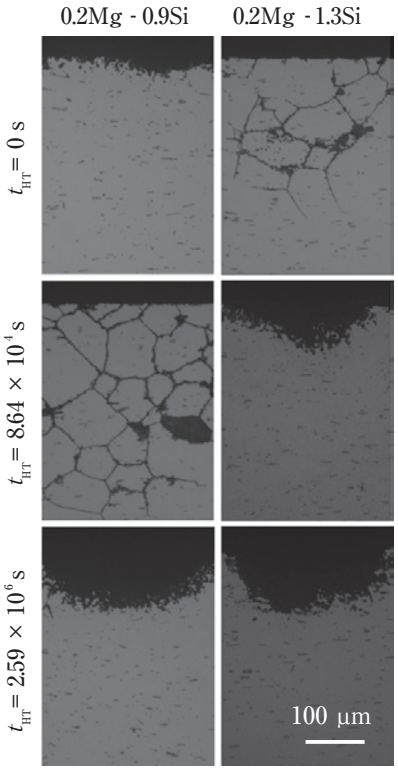

Fig. 4 Optical micrographs of the cross section after anodic dissolution for 0.2Mg-0.9Si and -1.3Si at $t_{HT} = 0$, 8.64×10^4 and 2.59×10^6 s.

and solid symbols show pitting corrosion and intergranular corrosion, respectively. Both the corrosion depth and corrosion morphology depended on HTT. For 0.2Mg-0.9Si, the corrosion morphology was pitting corrosion at $t_{HT} = 0$ and 7.20×10^3 s. The corrosion morphology was intergranular corrosion at $t_{HT} = 1.44 \times 10^4 - 3.46 \times 10^5$ s. The corrosion depth increased with increase in HTT and showed the maximum at $t_{HT} = 8.64 \times 10^4$ s. However, the intergranular corrosion was observed until $t_{HT} = 3.46 \times 10^5$ s and the corrosion depth decreased. The corrosion morphology was pitting corrosion again at $t_{HT} = 4.61 \times 10^5$ s. For 0.2Mg-1.3Si, the intergranular corrosion was observed at $t_{HT} = 0 - 2.88 \times 10^4$ s. The corrosion depth increased with HTT. The corrosion morphology was pitting corrosion at $t_{HT} = 8.64 \times 10^4$ s and corrosion depth decreased rapidly with HTT. That is, the susceptibility to intergranular corrosion of 0.2Mg-0.9Si and -1.3Si showed peak at $t_{HT} = 2.28 \times 10^4$ and 8.64×10^4 s, respectively.

3.2.2 TEM observation

Fig. 6 shows bright field TEM images of precipitates

on grain boundaries for 0.2Mg-1.3Si at $t_{HT} = 2.88 \times 10^4$ and 8.64×10^4 s. At $t_{HT} = 2.88 \times 10^4$ s, Si precipitates with diameter of about 4×10^{-8} m were observed on the grain boundary and could not be observed in the grain. A precipitate free zone (PFZ) along grain boundary was observed. At $t_{HT} = 8.64 \times 10^4$ s, Si precipitates with diameter of about 1×10^{-7} m on the grain boundary and about a few 10^{-8} m in the grain were observed. This indicates that Si precipitated and grew by the heat treatment at 453 K. PFZ was also observed at 8.64×10^4 s.

3.3 Al-1.1%Mn-Si alloys

3.3.1 Susceptibility to intergranular corrosion

Fig. 7 shows optical micrographs of the cross section after anodic dissolution for 1.1Mn-0.4Si, -0.8Si, and -1.4Si at $t_{HT} = 0$, 8.64×10^4, and 2.59×10^6 s. The corrosion morphology depended on Si concentration at $t_{HT} = 0$ s. Pitting corrosion was observed for 1.1Mn-0.4Si and -0.8Si and intergranular corrosion was observed for 1.1Mn-1.4Si. At $t_{HT} = 8.64 \times 10^4$ s, pitting corrosion was observed for 1.1Mn-0.4Si, intergranular corrosion was observed for 1.1Mn-0.8Si and -1.4Si. At $t_{HT} = 2.59 \times 10^6$ s, the corrosion morphology was pitting corrosion in each Si concentration.

Fig. 8 shows relationship between HTT and corrosion depth for 1.1Mn-0.4Si, -0.8Si, -1.2Si, and -1.4Si.

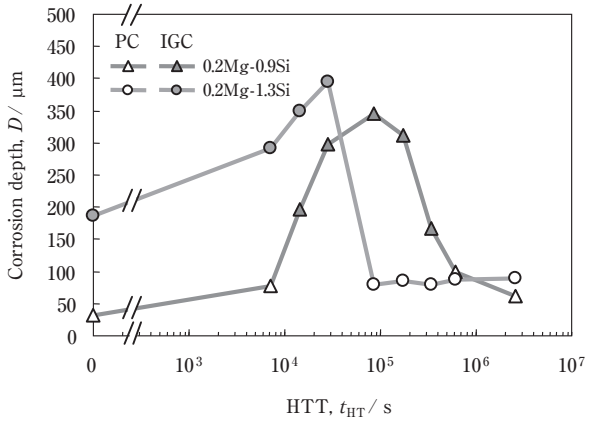

Fig. 5 Relationships between HTT and the corrosion depth for 0.2Mg-0.9Si and -1.3Si.
Pitting corrosion and intergranular corrosion are denoted as PC and IGC, respectively.

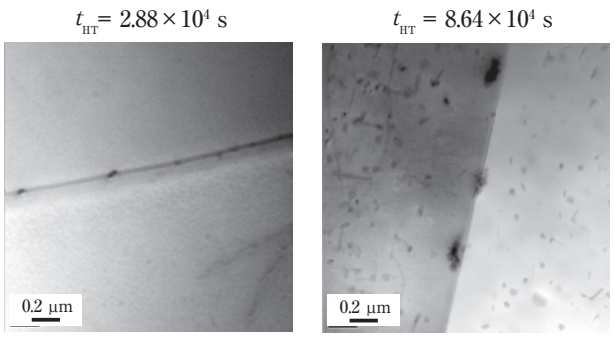

Fig. 6 Bright field TEM images of precipitates on grain boundaries for 0.2Mg-1.3Si at $t_{HT} = 2.88 \times 10^4$ and 8.64×10^4 s.

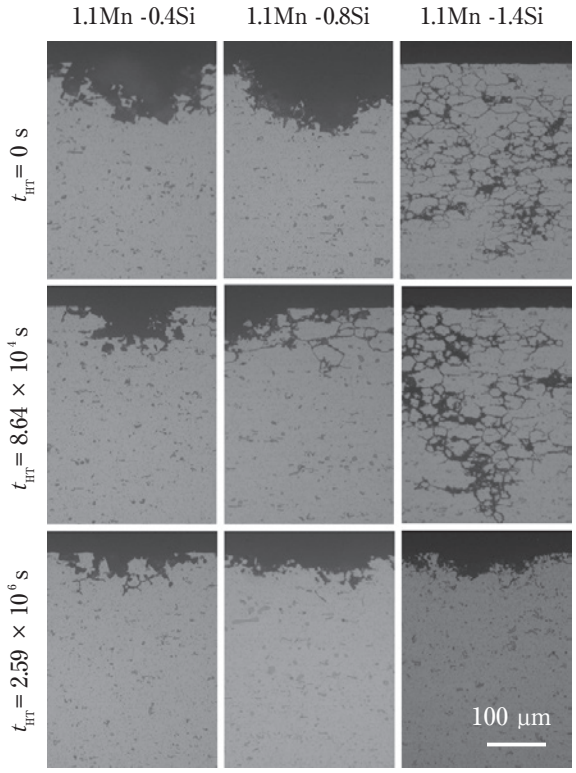

Fig. 7 Optical micrographs of the cross section after anodic dissolution for 1.1Mn-0.4Si, -0.8Si, and -1.4Si at $t_{HT} = 0$, 8.64×10^4, and 2.59×10^6 s.

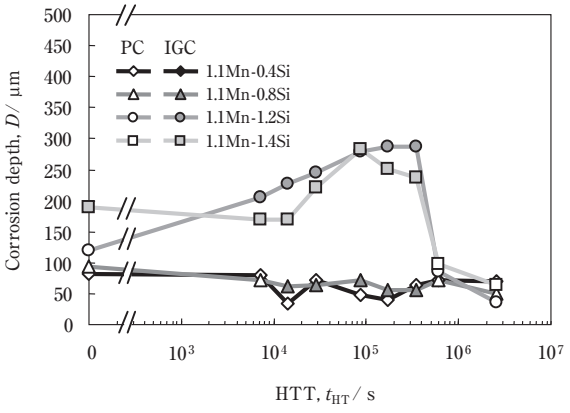

Fig. 8 Relationship between HTT and corrosion depth for 1.1Mn-0.4Si, -0.8Si, -1.2Si, and -1.4Si. Pitting corrosion and intergranular corrosion are denoted as PC and IGC, respectively.

The open and solid symbols show pitting corrosion and intergranular corrosion, respectively. The corrosion depth and morphology of 1.1Mn-0.4Si were independent of HTT while the corrosion depth and morphology of 1.1Mn-0.8Si, -1.2Si, and -1.4Si depended on HTT.

For 1.1Mn-0.8Si, corrosion morphology was pitting corrosion at t_{HT} = 0 and 7.20×10^3 s. and intergranular corrosion at t_{HT} = 1.44×10^4 s. Corrosion morphology was pitting corrosion again at t_{HT} = 6.05×10^5 s.

For 1.1Mn-1.2Si, the corrosion morphology was pitting corrosion at t_{HT} = 0 s and the intergranular corrosion at t_{HT} = 7.20×10^3 – 3.45×10^5 s. The Corrosion morphology was pitting corrosion again at t_{HT} = 6.05×10^5 s. The corrosion depth was the deepest at t_{HT} = 3.64×10^5 s and decreased with increase in HTT. For 1.1Mn-1.4Si, intergranular corrosion was observed at t_{HT} = 0 – 3.46×10^5 s, corrosion morphology was pitting corrosion at t_{HT} = 6.05×10^5 s. Corrosion depth was the deepest at t_{HT} = 8.64×10^4 s and then decreased rapidly with increase in HTT. That is, susceptibility to intergranular corrosion of 1.1Mn-1.2Si and -1.4Si showed a peak at t_{HT} = 3.46×10^5 and 8.64×10^4 s, respectively.

3.3.2 TEM observation

Fig. 9 shows bright field TEM images of precipitates on grain boundaries for 1.1Mn-1.2Si at t_{HT} = 0 and 7.20×10^6 s. Intermetallic compounds observed at t_{HT} = 0 s were Al-Mn series intermetallic compounds with gray spherical or elliptical shape. The distribution of Al-Mn series intermetallic compounds at t_{HT} = 7.20×10^6 s was the almost same to that at t_{HT} = 0 s. Dark black compounds were also observed on Al-Mn series intermetallic compounds, being Si precipitates identified by elemental analysis. It is suggested that Si precipitated and grew by the heat treatment at 453 K.

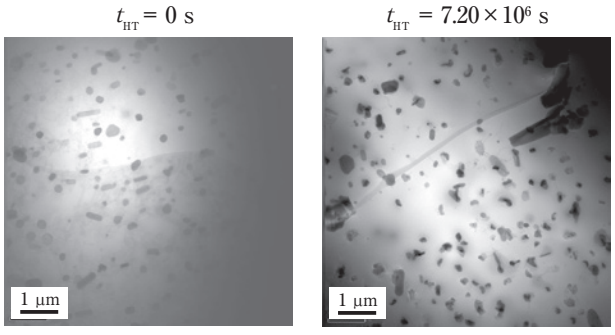

Fig. 9 Bright field TEM images of precipitates on grain boundaries for 1.1Mn-1.2Si at t_{HT} = 0 and 7.20×10^6 s.

3.4 Al-1.1%Mn-0.2%Mg-Si alloys

3.4.1 Susceptibility to intergranular corrosion

Fig. 10 shows optical micrographs of the cross section after anodic dissolution for 1.1Mn-0.2Mg-0.6Si, -0.8Si, and -1.4Si at t_{HT} = 0, 8.64×10^4, and 2.59×10^6 s. Corrosion morphology depended on Si concentration at t_{HT} = 0 s. Pitting corrosion was observed for 1.1Mn-0.2Mg-0.6Si and -0.8Si and intergranular corrosion was observed for -1.4Si. The pitting corrosion was observed for 1.1Mn-0.2Mg-0.6Si and intergranular corrosion for -0.8Si and -1.4Si at t_{HT} = 8.64×10^4 s. At t_{HT} = 2.59×10^6 s, the corrosion morphology was pitting corrosion in each Si concentration.

Fig.11 shows relationships between HTT and corrosion depth for 1.1Mn-0.2Mg-0.6Si, -0.8Si, -1.2Si, and -1.4Si. The open and solid symbols show pitting

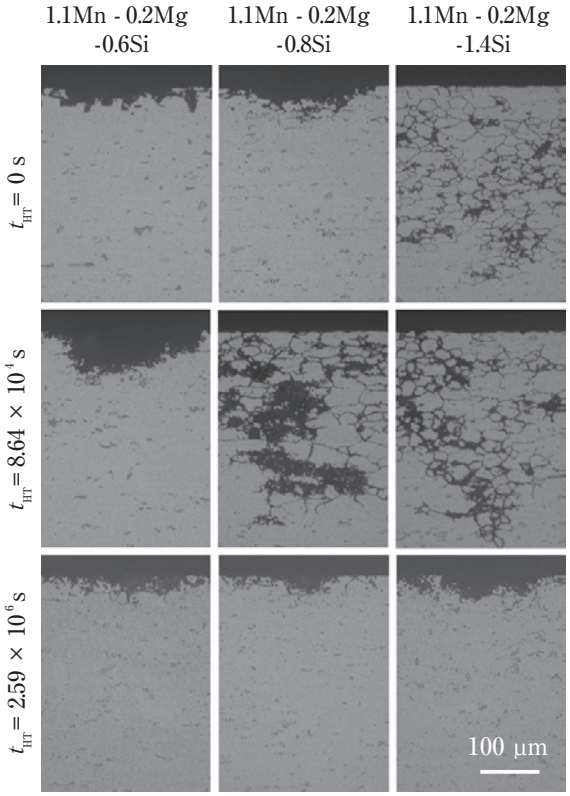

Fig. 10 Optical micrographs of the cross section after anodic dissolution for 1.1Mn-0.2Mg-0.6Si, -0.8Si, and -1.4Si at t_{HT} = 0, 8.64×10^4, and 2.59×10^6 s.

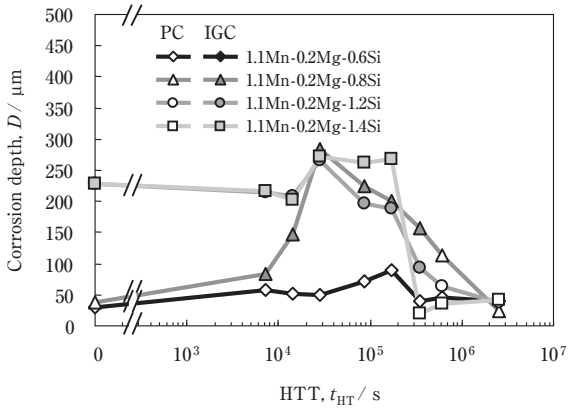

Fig. 11 Relationships between HTT and corrosion depth for 1.1Mn-0.2Mg-0.6Si, -0.8Si, -1.2Si, and -1.4Si. Pitting corrosion and intergranular corrosion are denoted as PC and IGC, respectively.

corrosion and intergranular corrosion, respectively. For 1.1Mn-0.2Mg-0.6Si, the corrosion depth was independent of HTT and the morphology was pitting corrosion in spite of HTT. The corrosion depth and morphology of 1.1Mn-0.2Mg-0.8Si, -1.2Si, and -1.4Si depended on HTT. For 1.1Mn-0.2Mg-0.8Si, corrosion morphology was pitting corrosion at $t_{HT} = 0$ s and intergranular corrosion at $t_{HT} = 7.20 \times 10^3$ s. Corrosion morphology was pitting corrosion again at $t_{HT} = 6.05 \times 10^5$ s. The corrosion depth at $t_{HT} = 2.88 \times 10^4$ s was the deepest within HTT. For 1.1Mn-0.2Mg-1.2Si, the intergranular corrosion was observed at $t_{HT} = 0 - 3.45 \times 10^5$ s. The corrosion morphology was pitting corrosion at $t_{HT} = 6.05 \times 10^5$ s. Corrosion depth at $t_{HT} = 2.88 \times 10^4$ s was the deepest. For 1.1Mn-0.2Mg-1.4Si, intergranular corrosion was observed at $t_{HT} = 0 - 1.73 \times 10^5$ s, corrosion morphology was pitting corrosion at $t_{HT} = 3.46 \times 10^5$ s. Corrosion depth at $t_{HT} = 3.46 \times 10^4$ s was the deepest and then the corrosion depth decreased rapidly. That is, susceptibility to intergranular corrosion of 1.1Mn-0.2Mg-0.8Si, -1.2Si, and -1.4Si showed peak at $t_{HT} = 2.88 \times 10^4$ s.

4. Discussions

As shown in Fig. 1 and Fig. 2, 0.4Si did not have intergranular corrosion susceptibility regardless of HTT. Al-Si alloy containing more than 0.4%Si showed the intergranular corrosion at $t_{HT} \geq 0$ or 8.64×10^4 s. It is clear that the susceptibility to intergranular corrosion increased with increase in Si concentration. Therefore the intergranular corrosion which occurred at $t_{HT} = 0 - 2.59 \times 10^6$ s was caused by Si. Because solute Si makes E_{PIT} of aluminum noble as well as solute Cu[12], it is thought that a mechanism of generation of susceptibility to the intergranular corrosion caused by Si is the same as that caused by Cu. According to the mechanism about the generation of the intergranular corrosion in Al-Cu alloys, the intergranular corrosion is preferential corrosion on grain boundaries caused by difference of E_{PIT} between a grain and Cu depleted layer along a grain boundary. Thus, it is suggested that the intergranular corrosion in Al-Si alloys is generated by the Si depleted layer along a grain boundary. It is expected that corrosion depth of intergranular corrosion will increased with Si concentration because of formation of continuous Si depleted layer and increase in difference of E_{PIT} between grain and Si depleted layer along grain boundary leading to preferential dissolution of grain boundaries. This tendency was found in Fig. 2. As shown in Fig. 2, corrosion depth increased once and turned to decrease with HTT. This mechanism, in which corrosion depth had such HTT dependence, is thought as following. Si precipitates on grain boundaries at cooling process after brazing and heat treatment at 453 K, and Si depleted layer along grain boundaries is formed continuously. The continuous Si depleted layer causes intergranular corrosion. However, the heat treatment for a long time not only precipitates on grain boundaries but also in grain caused to decrease in solute Si concentration. The Si concentration in the grain continues to decrease until attaining to the concentration on the grain boundary. It means that the pitting potentials in the grain and the grain boundary become the same. Thus, corrosion progresses in both the grain and the grain boundary, indicating that the corrosion depth decreases and the susceptibility to intergranular corrosion disappear. To confirm mechanism, **Fig. 12** shows STEM-EDS line analysis for Si on grain boundary for 1.4Si at $t_{HT} = 0$ and 2.59×10^6 s. At $t_{HT} = 0$ s, Si intensity decreased around grain boundary. The decrease in Si intensity corresponded to Si depleted layer along a grain boundary. At $t_{HT} = 2.59 \times 10^6$ s, deference in Si

intensity between grain and grain boundary was not observed.

As shown in Fig. 6 and Fig. 9, regardless of alloy elements, precipitation and growth of Si precipitates occurred by the heat treatment at 453 K. It is thought that generation and disappearance of the intergranular corrosion were caused by Si depleted layer along a grain boundary for Al-0.2%Mg-Si alloys as mentioned in 3.2, Al-1.1%Mn-Si alloys in 3.3, and Al-1.1%Mn-0.2%Mg-Si alloys in 3.4 in the same as Al-Si alloys. **Fig. 13** shows relationships between HTT, when corrosion depth is the deepest, or corrosion morphology changes from intergranular corrosion to pitting corrosion, and Si concentration for specimens. HTT, when corrosion depth is the deepest or corrosion morphology changes from intergranular corrosion to pitting corrosion, little depended on Si concentration. These were the longest for Al-Si alloys and were shortened by other alloy element. This is reason why the addition of Mn and Mg induces promoted precipitation of some kinds of intermetallic compounds. These intermetallic compounds promoted precipitation of Si precipitates because these intermetallic compounds became a nucleation site.

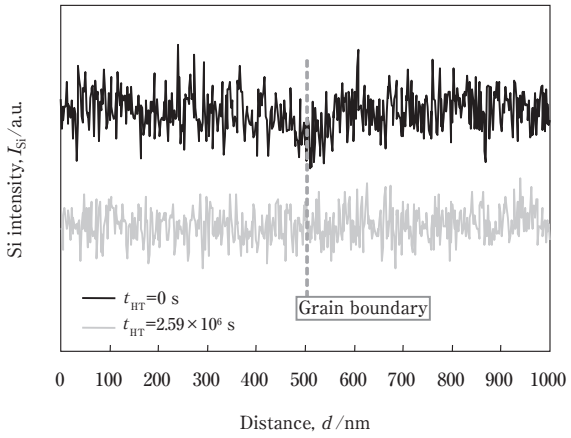

Fig. 12 STEM-EDS line analysis for Si on a grain boundary for 1.4Si at t_{HT} = 0 and 2.59 × 10^6 s.

5. Conclusions

We investigated that susceptibility to intergranular corrosion of Al-Si alloys, Al-0.2%Mg-Si alloys, Al-1.1%Mn-Si alloys and Al-1.1%Mn-0.2%Mg-Si alloys heat-treated at 453 K after brazing process. For a mechanism of generation and disappearance of susceptibility to intergranular corrosion, following conclusions were drawn.

(1) Addition of Si caused susceptibility to intergranular corrosion for each alloy series. Susceptibility to intergranular corrosion was observed for the as-brazed specimen containing higher than 1.2%Si.

(2) Susceptibility to intergranular corrosion increased with increase in the heat treatment time at 453 K once, but turned to decrease.

(3) Short heat treatment at 453 K caused precipitation and growth of Si precipitates on grain boundaries and then continuous Si depleted layer along grain boundaries was formed. Si precipitates were also precipitated

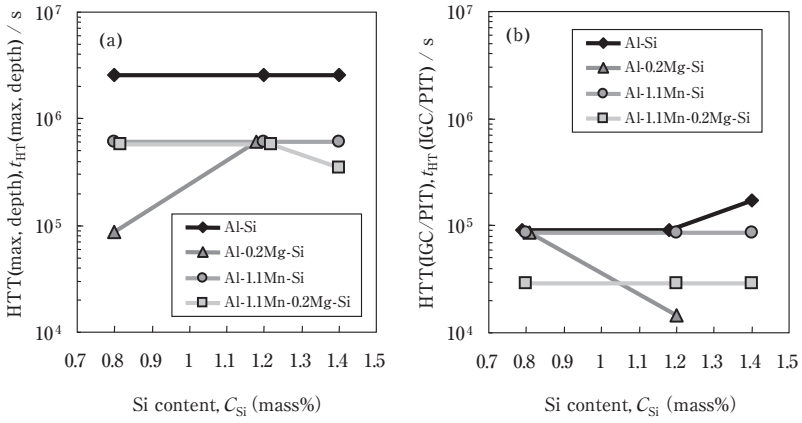

Fig. 13 Relationships between HTT, when (a) corrosion depth is the deepest, or (b) corrosion morphology changes from intergranular corrosion to pitting corrosion, and Si concentration for specimens.

in grain at long term heat treatment at 453 K, solute Si concentration in a grain decreased to that on a grain boundary. This is reason why the susceptibility to intergranular corrosion had time dependence.

(4) Addition of Mg and Mn promoted generation of susceptibility to intergranular corrosion because Mg_2Si intermetallic compounds and Al-Mn series intermetallic compounds promoted precipitation of Si precipitates.

(5) Addition of Mg and Mn promoted disappearance of susceptibility to intergranular corrosion the same as generation.

References

1) J. K. Kunesch: Proceedings of the 2nd International Congress Aluminium Brazing, (Aluminium Verl., Hotel Nikko, Düsseldorf, 2002), pp. 15-17.
2) M. Kaifu, H. Fujimoto and M. Takemoto: J. Japan Inst. Met. **32** (1982), 135-142.
3) K. Tohma: J. Japan Inst. Met. **36** (1986), 89-98.
4) M. Zamin: Corrosion **37** (1981), 627-632.
5) J. R. Galvele and S. M. De De Michel: Corros. Sci. **10** (1970), 795-807.
6) M. H. Larsen, J. C. Walmsley, O. Lunder and K. Nisancioglu: J. Electorchem. Soc. **157** (2010), C61-C68.
7) K. Tohma, Y. Sugai and Y. Takeuchi: J. Japan Inst. Met. **31** (1981), 157-163.
8) K. Tohma: J. Japan Inst. Met. **34** (1984), 351-360.
9) K. Yamaguchi and K. Tohma: J. Japan Inst. Met. **47** (1997), 285-291.
10) S. Iwao and M. Asano: J. Japan Inst. Met. **59** (2009), 108-113.
11) S. Iwao, M. Edo and S. Kuroda: J. Japan Inst. Met. **60** (2010), 327-332.
12) J. R. Davis: Corrosion of Aluminum and Aluminum Alloys, (ASM International, Ohio, 1999), pp. 28.

Yoshiyuki Oya

No. 2 Department, Fukaya Center, Research & Development Division, UACJ Corporation

Yoichi Kojima

No. 2 Department, Fukaya Center, Research & Development Division, UACJ Corporation